Ulrich Messerschmidt[a], Martin Bartsch[a], Christian Dietzsch[a], Wolfgang Kurtz[b], Christina Scheu[b,c], Manfred Rühle[b]

[a] Max-Planck-Institut für Mikrostrukturphysik, Halle (Saale), Germany
[b] Max-Planck-Institut für Metallforschung, Stuttgart, Germany
[c] Materialprüfungsanstalt, Universität Stuttgart, Stuttgart, Germany

HVEM in situ study of fracture of Al_2O_3/Nb sandwich specimens

In situ straining experiments on α-Al_2O_3/Nb/α-Al_2O_3 single crystal sandwiches have been performed in a high-voltage electron microscope in order to observe the dislocation motion connected with the fracture of these samples. The tricrystals had two different orientation relationships at the interfaces, both possessing high fracture energies. The *in situ* studies showed that the fracture occurs along the interfaces but more frequently inside the Nb sheet. The fracture is connected with strong plastic deformation. The crack opening and the dislocation processes are analysed.

Key words: Metal/ceramic interfaces; In situ fracture in TEM; Plastic fracture; Crack opening displacement

1. Introduction

The mechanical properties of metal/ceramic composites are critically depending on the fracture behaviour of the interfaces. Since both constituents of these composites have quite different elastic and plastic properties, the fracture processes along or near the interfaces may considerably differ from those in homogeneous materials. The fracture along the interfaces is controlled by the work of adhesion W_{ad}. However, the total fracture energy J_c may be higher than the work of adhesion by more than three orders of magnitude. For a review see [1]. This difference results from the occurrence of plastic deformation both near the crack which increases the fracture toughness as well as far from the crack.

If the stress intensity factor at the crack is high enough, new dislocations can be nucleated at the crack tip. The Rice–Thomson model for homogeneous solids [2] has been extended for bi-materials in [3]. Finally, dislocation nucleation at an interface crack is described by a Peierls-type model [4]. In addition to the direct dislocation nucleation, dislocations can also be generated in the plastic zone of a crack by dislocation multiplication [5–7] as during plastic deformation of homogeneous materials. Although the role of plastic deformation for interface fracture is recognized, experimental studies on dislocation creation and motion during deformation processes are only rarely reported.

α-Al_2O_3/Nb bi-crystals can be produced by ultra-high vacuum diffusion bonding with geometrically and chemically well defined interfaces. They have been thoroughly investigated (e. g., [8–11]) and are therefore well suited to serve as a model system for interface fracture studies. In the present paper, *in situ* deformation inside a high-voltage electron microscope (HVEM) is performed to investigate the processes of plastic deformation in connection with the fracture of α-Al_2O_3/Nb bi-crystals. By this method, the dislocation motion can directly be observed.

2. Specimen and deformation geometry

The specimens were obtained from several composite blocks consisting of a Nb single crystal sheet of about 2 mm thickness joined to two α-Al_2O_3 single crystal pieces. The two different interfaces had the following orientation relationships (OR)

OR A: $(110)_{Nb} \parallel (0001)_{Al2O3}$, $[1\bar{1}0]_{Nb} \parallel [01\bar{1}0]_{Al2O3}$

OR B: $(110)_{Nb} \parallel (0001)_{Al2O3}$, $[1\bar{1}0]_{Nb} \parallel [2\bar{1}\bar{1}0]_{Al2O3}$

During the *in situ* straining experiments, the micro-tensile specimens were loaded along the interface normal, i. e. along $[110]_{Nb}$. The samples were cut with two different orientations of the foil normal relative to the Nb:

(1) with $[1\bar{1}0]_{Nb}$ foil normal

(2) with $[001]_{Nb}$ foil normal.

Thus, in total four different TEM specimens were prepared, two for each interface. These are named A1 ... B2 as shown in Fig. 1.

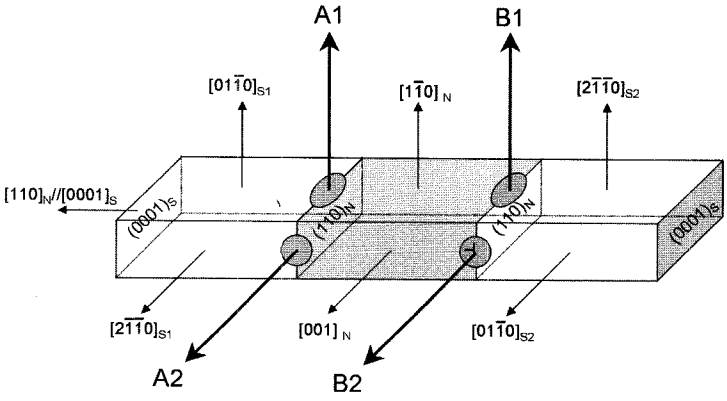

Fig. 1. Orientation relationships of the Al_2O_3/Nb/Al_2O_3 tricrystals including the foil normals of the microtensile specimens.

Table 1. Slip systems with non-zero orientation factors in Nb loaded along [110].

Burgers vector	slip plane	orientation factor
1/2[111]	$(01\bar{1})$	0.408
	$(10\bar{1})$	0.408
	$(11\bar{2})$	0.471
	$(\bar{1}2\bar{1})$	0.236
	$(2\bar{1}\bar{1})$	0.236
1/2[11$\bar{1}$]	(011)	0.408
	(101)	0.408
	(112)	0.471
	$(\bar{1}21)$	0.236
	$(2\bar{1}1)$	0.236

The deformation of the Nb crystals is carried by dislocations with $1/2\langle 111\rangle$ Burgers vectors on {110} and {112} planes [12]. Two of the four $1/2\langle 111\rangle$ Burgers vectors are parallel to the interface plane. Since this plane is perpendicular to the tensile direction, the orientation factors of the corresponding slip systems are zero. The slip systems with non-zero orientation factors are listed in Table 1. For specimens with foil normal 1, the Burgers vectors are parallel to the foil plane and have angles of 35.3° with the tensile axis. They also mark the directions of the traces of the slip planes. The different planes are characterized by different widths of the slip traces. For specimens with foil normal 2, the traces of the {110} slip planes have angles of 45° with the tensile direction. The traces of the {112} planes are either perpendicular to or have angles of 18.4° with the tensile direction. Thus, the planes can be identified by the orientations of the traces only. In some cases, also slip systems with macroscopically zero orientation factors were observed.

3. Experimental

Pure α-Al_2O_3 and Nb single crystals were diffusion bonded in ultra-high vacuum using the procedure as in [10] with the orientation relations described above. The bonding was performed at a temperature of 1400 °C and a load of 7 MPa for 3 hours. In addition to the single-crystal samples, preliminary experiments were performed using sandwich specimens with a polycrystalline Nb sheet.

Micro-tensile specimens for the *in situ* straining experiments in the HVEM were prepared in the following way. From the bonded sandwiches, slices about $8 \times 2 \times 0.3$ mm^3 in size were cut by a wire saw. The slices were ground using a suspension of 3 μm diamond powder in oil on a brass plate and afterwards carefully polished with 1 μm diamond paste on a special plastic foil. In order to ob-

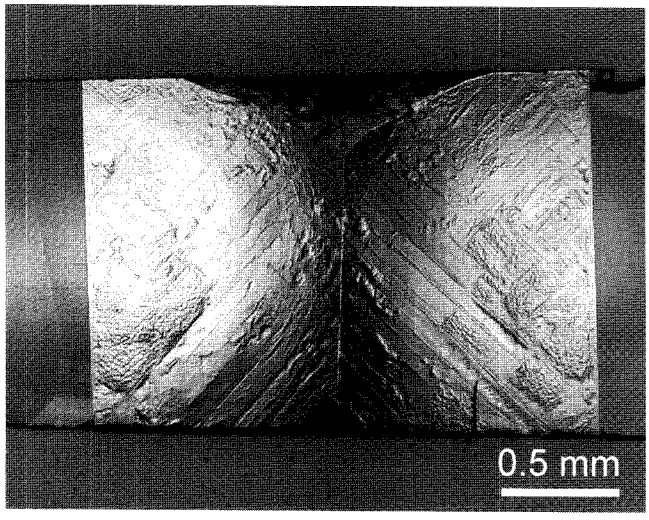

Fig. 2. Optical micrograph of the central part of a micro-tensile specimen.

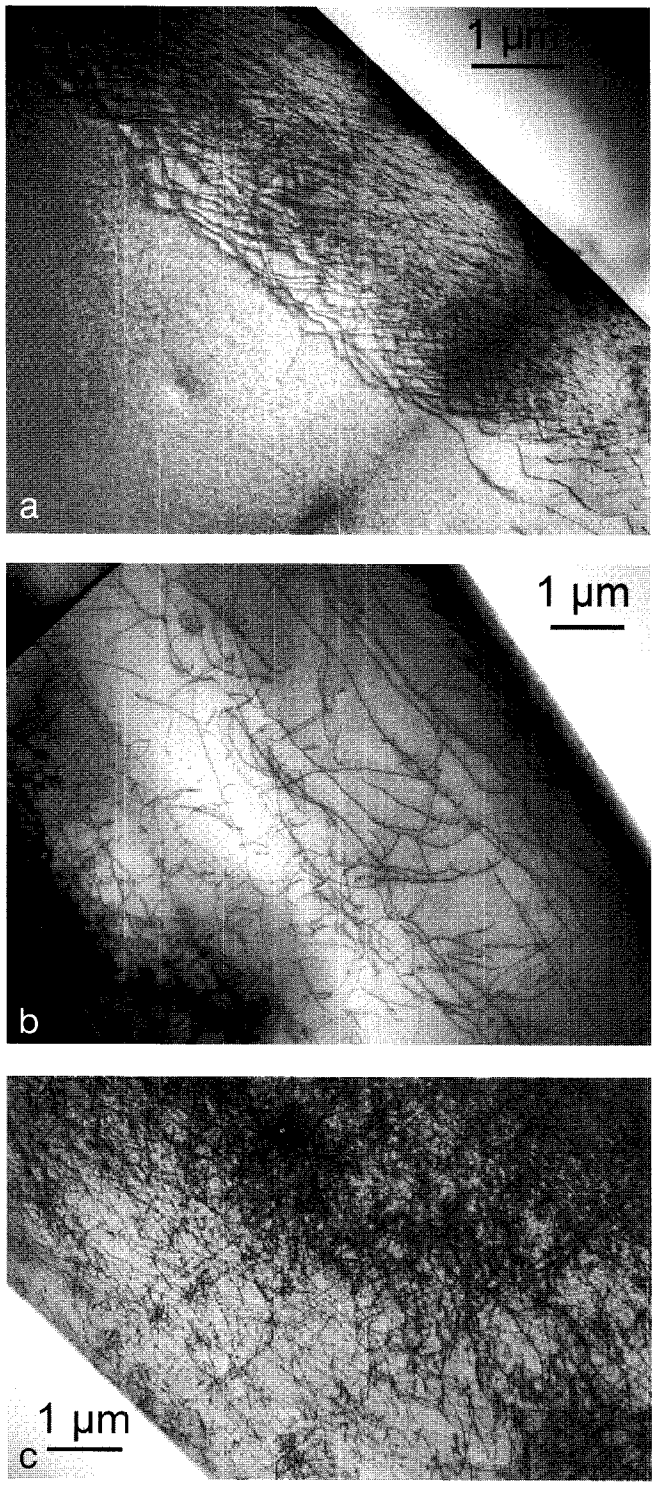

Fig. 3. Dislocation structures produced during the bonding procedure. a) Dislocations near the interface. b) Relatively homogeneous distribution of dislocations of low density. c) Dense dislocation network.

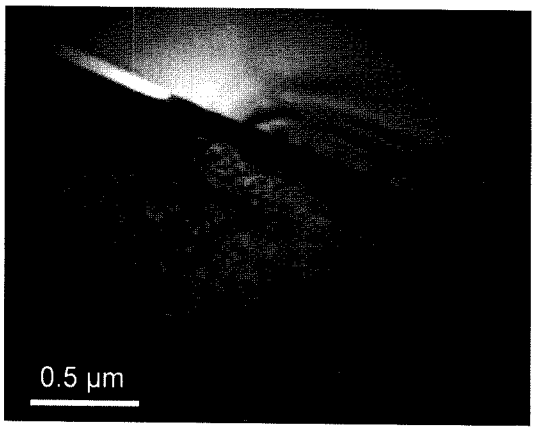

Fig. 4. Video frame of a crack growing slowly along the interface of OR A2.

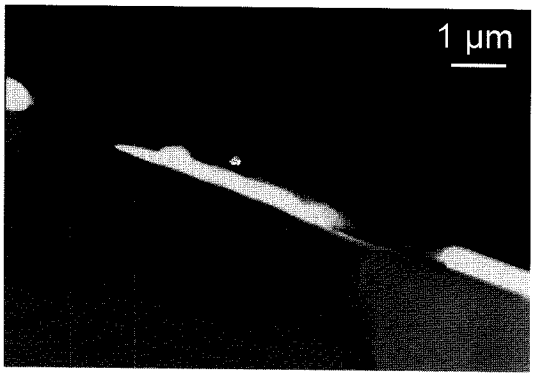

Fig. 5. A crack growing along the interface by void formation and coalescence in a specimen with a polycrystalline Nb sheet.

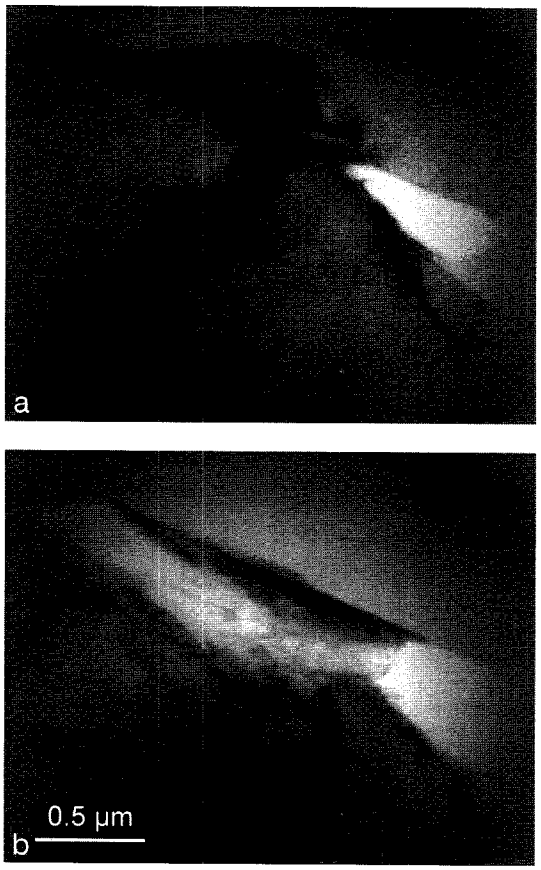

Fig. 6. Two stages of a video recording taken of a specimen of OR B1 showing the transfer of a crack growing along the interface into the Nb connected with crack blunting and formation of voids in front of the crack.

serve the dislocation motion in the Nb sheet near the interface, the transparent area of the specimens had to be placed in this region. Unfortunately, the Nb is much less transparent for electrons than the Al_2O_3. Therefore, the area of interest was pre-thinned by mechanical dimpling. Dimples were placed on both interfaces, either three usual spherical dimples along each interface or one at each interface using a special dimpler. The latter allowed an additional translational movement to produce large dimples with a flat bottom as imaged in Fig. 2. A serious problem of the dimpling was the higher thinning rate of Nb with respect to Al_2O_3. This effect was not observed in preliminary tests with polycrystalline Nb sheets of only 0.3 to 0.6 mm thickness where the dimpling wheels are supported on both Al_2O_3 pieces neighbouring the Nb sheet. The effect can be reduced by using hard dimpling wheels. The thickness of the dimple bottoms in the Al_2O_3 can be estimated from Newton fringes which, however, requires polished surfaces. Therefore, dimpling wheels from wood were used as a compromise. In addition, the centres of the dimples were first placed about 10 µm away from the interface into the Al_2O_3 and only after the occurrence of Newton fringes shifted to the interface.

The final thinning was performed by Ar^+ ion milling with an angle of incidence around 15°. Here, higher thinning rates of the Nb compared to Al_2O_3 were also observed. Therefore, the ion beam was focussed on the interface from the Nb side. This yielded several perforations along the interface and a surface structure with elongated dimples. After ion milling, band-like structures occurred on the surface of the Nb as demonstrated in Fig. 2, independent of the thinning rates. These structures correspond to slip bands originating from plastic deformation during the diffusion bonding process. According to the shape of excess Nb standing out of the Al_2O_3 plates during bonding, the plastic strain reached several percent.

The *in situ* straining experiments were performed in a quantitative double-tilting tensile stage [13] in an HVEM operated at 1 MeV. The stage allowed a well defined digital control and recording of the specimen load and elongation. The microscope was attached with a video camera which allowed the acquisition of real-time videos during the straining experiments. The video clips were analysed frame by frame. At certain stages of the straining experiments, additionally photographic micrographs were recorded which have a higher quality compared to the video frames.

4. Results

4.1. Initial dislocation structure in the Nb prior to the *in situ* straining

As described above, the Nb component of the sandwich specimens undergoes plastic deformation during the diffusion bonding process. This results in the generation of a dislocation structure, which impairs the observation of the plastic deformation during the *in situ* straining. Figure 3 shows that the dislocation structures are (a) sometimes re-

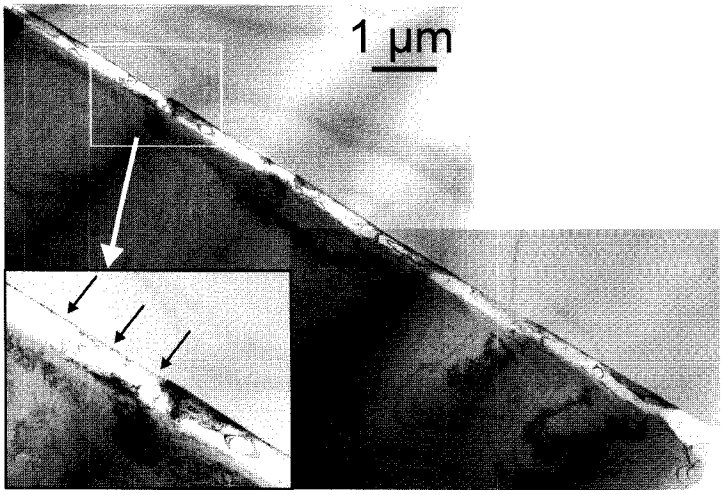

Fig. 7. Photographic micrographs taken at a later stage after the video recording of Fig. 6.

stricted to the vicinity of the interface, (b) sometimes extend quite far into the bulk of the Nb sheet and (c) may have a high dislocation density.

4.2. Crack path and shape

In total, there were two experiments performed successfully on the sandwich specimens with polycrystalline Nb sheets and six ones on such with Nb single crystals, mostly of OR B. Only in two of these specimens, the crack runs along the interface, in two others it proceeded inside the Nb near the interface but in four specimens the crack grew in the Nb far from the interface.

Figure 4, taken from a video recording, presents a crack growing slowly along the interface in a specimen of OR A2. As described above, the macroscopic tensile stress acts always perpendicular to the interface in $[110]_{Nb}$ direction. The crack moves with considerable plastic deformation in the Nb leading to crack blunting. A later stage of this type of motion is shown in Fig. 5, observed in a specimen with a polycrystalline Nb sheet. Voids have grown in front of the main crack and the failure proceeds by the coalescence of these voids. In the frames of Fig. 6, taken from a video sequence, the crack grows first slowly along the interface accompanied with some blunting. Afterwards, it leaves the interface and proceeds in the Nb. At this time, extensive plastic deformation starts. Suddenly, the displacement of the crack faces increases. This is connected with the formation of strongly thinned areas containing voids. A later stage is shown at a better resolution in the micrographs in Fig. 7, which were recorded on photographic film. The crack is formed mainly in the Nb. However, there are also several regions of decohesion at the interface. One is demonstrated in the magnified inset, which shows an enlarged section of the micrograph. These microcracks along the interface show a step in the Nb at the backward (right) side and are sharp in the forward direction of crack motion. One example of a crack moving completely in the Nb sheet is demonstrated in Fig. 8. The crack is connected with heavy plastic deformation and its tip has branched.

From the shape of the cracks along the interface in Figs. 4, 5, and 6b, the crack opening displacement (COD) δ_c can be measured. It amounts to about 70 nm for the crack in Fig. 4 and about 360 nm for the cracks in Figs. 5 and 6b. In homogeneous materials, the crack opening displacement allows to determine the energy release rate G_{cCOD} [14]

$$G_{cCOD} = m\delta_c\sigma_y \quad (1)$$

where m is a numerical factor with $1 < m < 3$ and σ_y is the yield stress of the material. In a first approximation, it is assumed that this relation holds also for fracture along or near the interface. The yield stress of Nb was measured along the $\langle 110 \rangle$ direction characteristic of the present loading conditions on the excess material of a sandwich specimen with the same thermal history as the present specimens yielding $\sigma_y = 84$ MPa [15]. With this value and an intermediate value of $m = 2$, G_{cCOD} amounts to about 12 J m^{-2} for the specimen in Fig. 4 and 60 J m^{-2} for the specimens in Figs. 5 and 6b. The large opening of the crack inside the Nb in Fig. 8 cannot be used to calculate G_{cCOD} since further crack growth is controlled by the tips of the small branches in front of the main crack.

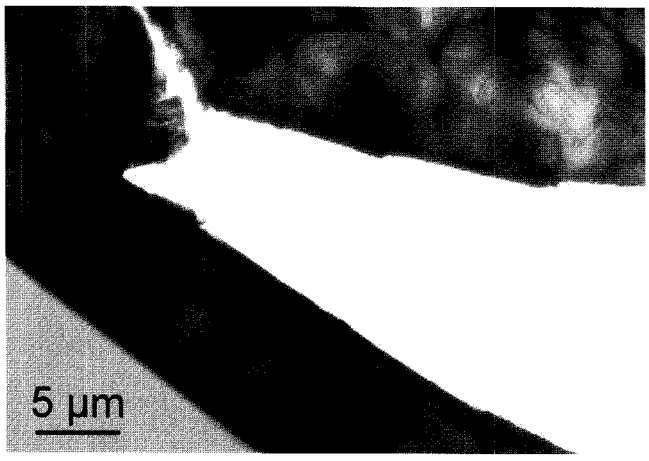

Fig. 8. Crack in a specimen of OR B1 with branched tip in the Nb.

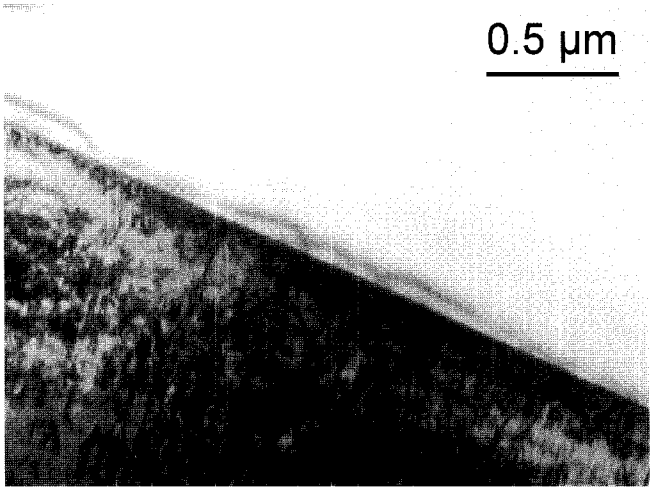

Fig. 9. Contrast fringes in the Al_2O_3 near the interface during *in situ* loading of a sandwich specimen with polycrystalline Nb sheet.

4.3. Plastic deformation processes

As described in Section 4.1., the plastic deformation processes connected with the fracture are impaired by the dislocation structures resulting from the diffusion bonding process. Nevertheless, the crack-induced dislocation motion can be identified during the dynamic observation in the *in situ* straining experiments in the HVEM.

During the elastic loading of the *in situ* specimens, before dislocation motion was observed, contrast fringes appear in the Al_2O_3 crystals near the interface (Fig. 9). The contrasts consist of small bright dots along the interface with distances between about 35 and 70 nm. In between these dots dark contrast fringes occur. The contrast features are still visible during plastic deformation as demonstrated in Figs. 14 to 16 below.

Most slip systems described in Section 2 and Table 1 are observed in the experiment. This can be seen most clearly in regions of plastic deformation near the interface but far away from the crack. Figure 10 presents the case of the $[1\bar{1}0]_{Nb}$ viewing direction (OR B1) with the two active Burgers vectors $1/2[111]$ and $1/2[11\bar{1}]$ in the foil plane. The Burgers vectors were determined by contrast extinction experiments using the $\mathbf{g} \cdot \mathbf{b} = 0$ rule. The dislocations are elongated along the Burgers vector directions, i. e. they are mainly screw dislocations. Since the width of the slip traces is small, the slip planes are most likely the $(11\bar{2})$ and (112) planes imaged edge on. These slip systems have maximum orientation factors $m_s = 0.471$. In addition, dislocations were observed having Burgers vectors in the interface plane with zero orientation factors. An example is shown in Fig. 11, which was taken at a similar area of the same specimen. Dislocations labelled by arrows move along traces perpendicular to the interface plane. The corresponding slip planes do not contain the directions of the Burgers vectors listed above but those with zero orientation factors.

The dislocation structure of a specimen with OR A2 is displayed in Fig. 12. The dislocations belong to a slip plane which has traces parallel to the trace of the interface, i. e. the (112) or $(11\bar{2})$ plane with the maximum orientation factor of 0.471. The Burgers vectors point out of the interface plane. Other dislocations in this specimen move on the $(01\bar{1})$ plane with $m_s = 0.408$. However, again dislocations are observed moving on planes which do not contain the

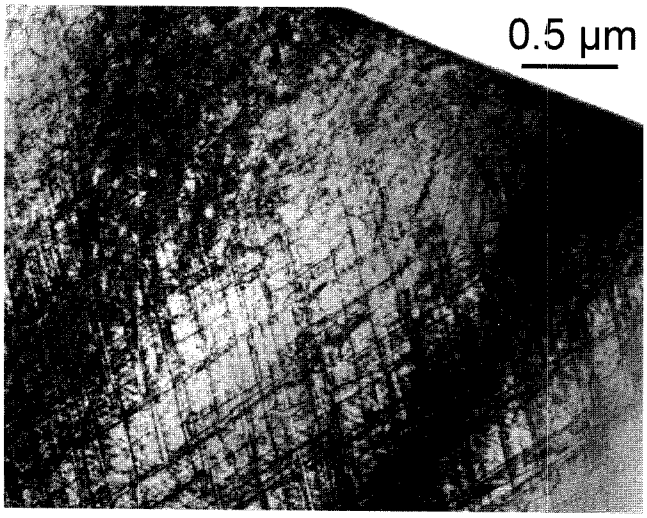

Fig. 10. Dislocation structure generated during *in situ* deformation of a specimen of OR B1 with Burgers vectors in the foil plane.

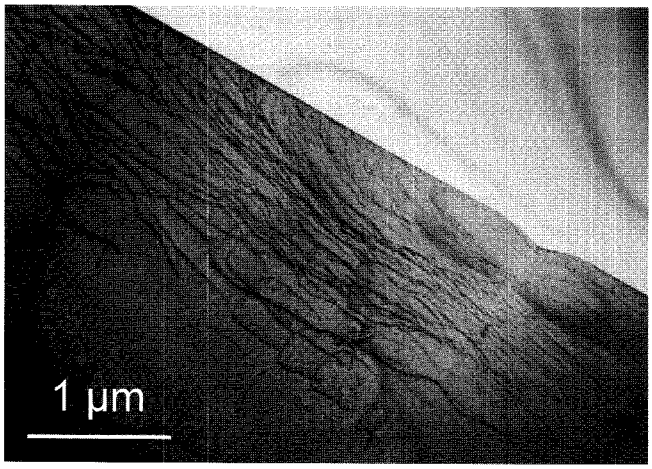

Fig. 12. Dislocations moving in a specimen of OR A2 on a plane with a trace parallel to the interface plane.

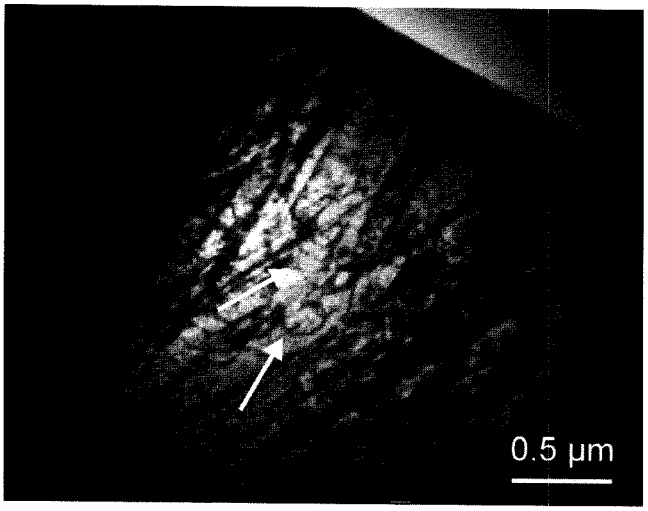

Fig. 11. Video frame of the same specimen as Fig. 10 with dislocations moving on traces perpendicular to the interface, i. e. with Burgers vectors in the interface plane.

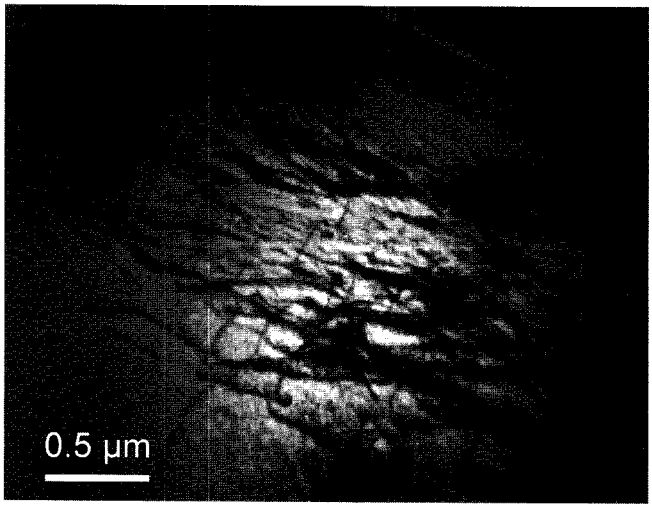

Fig. 13. Frame from a video recording with dislocations moving in a specimen of OR A2 close to (121) planes.

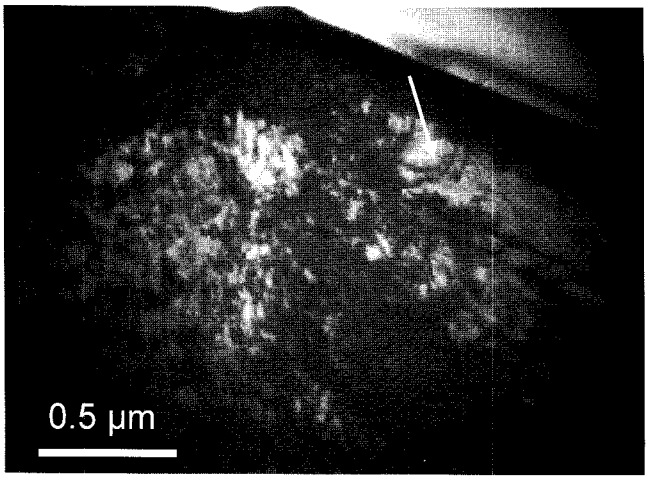

Fig. 14. Frame from a video recording with dislocations moving away from the crack (arrow) in a specimen with OR A2.

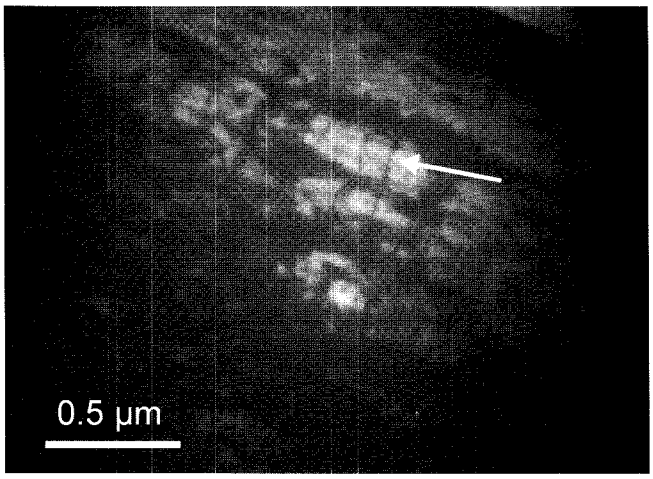

Fig. 15. Frame from a video recording of an area slightly right of that of Fig. 14 with dislocations moving towards the crack.

two Burgers vectors yielding orientation factors different from zero. An example is presented in Fig. 13 where the dislocations move on (121) planes.

Thus, in general the stress state near the interface is complex. In addition to dislocations which move with large orientation factors in a macroscopic sense, also dislocations on slip systems with zero orientation factors occur. Frequently, the traces are not straight indicating extensive cross slip. Most dislocations move away from the interface but some dislocation motion was observed in the opposite direction, too. The dominating slip planes are of the {112} type.

Plastic deformation is particularly extensive near the crack tips. Since the dislocation density is high in these regions and since the structures are superimposed with bending contours, details of the dislocation motion are difficult to observe. Many dislocations are created near the crack and move away from it as illustrated in Fig. 14. The dislocations bow out in the forward direction of motion and move on (112) or $(11\bar{2})$ planes with the maximum orientation factor of 0.471. Figure 15 presents an area at a slightly larger distance from the same crack. In this case, the dislocations move towards the crack on the same types of planes. Thus, in the plastic zones of the cracks dislocations of both signs are observed suggesting that the dislocations are not emitted from the crack but are generated by dislocation multiplication. Since the stresses are higher near the crack, more dislocations move away from the crack than towards it. Figure 16 shows that the multiplication takes place by the usual double-cross slip (Koehler–Orowan–Gilman) multiplication process [5–7]. In Fig. 16a, a dislocation has formed a small dislocation dipole at a jog. The respective dislocation is marked by an arrow and drawn schematically at the upper right corner of the micrograph. On further motion of the dislocation, the dipole opens (Fig. 16b) and the dislocation obtains a shape like a φ. Between Figs. 16b and e, the new loop at the right side of the φ grows. In Fig. 16f, the loop is terminated and the original dislocation has moved away. Finally, two new dislocations move away (not shown in the figure).

To summarize, extensive plastic deformation occurs near the crack tip but also quite far away from it. Many dislocations move on planes of {112} type with high macroscopic orientation factors. Near the interface, dislocations move also on planes containing the Burgers vectors in the interface, i. e. on slip systems with zero macroscopic orientation factors, indicating a complicated stress state. Most dislocations are created by the double-cross slip multiplication mechanism.

5. Discussion

Interfaces with the orientation relationships used in the present work, have the highest fracture energies of about 1900 J m^{-2}. This was measured on single-ended notched beam bending specimens in previous studies [10, 11, 16–18]. Values between 760 and 2300 J m^{-2} were determined by the present authors on chevron-notched bending bars [15]. The present *in situ* study indicates that the cracks run sometimes along the interface but in most cases inside the Nb sheet. This is in contrast to observations of the chevron-notch fracture tests, where the cracks run mostly close to the interface but in the sapphire. According to the linear elastic fracture theory including small scale yielding [19, 20], the crack path is determined by the second Dundurs' parameter β, defined by [21]

$$\beta = \frac{\mu_1(1-2\nu_2) - \mu_2(1-2\nu_1)}{\mu_1(1-\nu_2) + \mu_2(1-\nu_1)} \qquad (2)$$

μ_i and ν_i are the shear moduli and Poisson's ratios of the constituents of the specimens. In the present case of a strong interface and $\beta > 0$ ($\beta = 0.214$ for OR B [10]), a crack running in the sapphire should be attracted towards the interface. That the cracks in most cases do not run along the interface is certainly caused by the particular specimen geometry. The specimen thickness along the electron beam direction is typically less than 500 nm and thus small compared to other specimen dimensions, e. g. the thickness of the metal layer or the specimen width. Besides, the cross section of the specimens is not homogeneous. Most probably, the Nb sheet is thinner than the neighbouring sapphire, so that the crack follows the path of lowest crack resistance.

In all cases, i. e., when the crack runs along the interface or inside the Nb, the crack tip is blunted indicating strong plastic deformation (see Figs. 4 to 6 for the cracks along the interface). The energy release rates G_{cCOD} from Eq. (1), which correspond to the observed crack opening displacements, amount to 12 J m^{-2} for the crack in Fig. 4

with OR A and to 60 J m^{-2} for that in Fig. 6b with OR B. These values can be compared with the work of adhesion W_{ad} and with the macroscopically measured fracture energies. W_{ad} amounts to only 0.49 J m^{-2} for OR A and to 0.95 J m^{-2} for OR B ([22], quoted in [1]). The present G_{cCOD} values scale with W_{ad} but are more than an order of magnitude higher due to the plastic deformation near the crack tip. Average values of G_c determined from the stress intensity factors in chevron-notch bending tests amount to 313 and 426 J m^{-2} [15]. Thus, macroscopic specimens are stronger than it is indicated by the crack opening during the *in situ* straining experiments. The average total work of

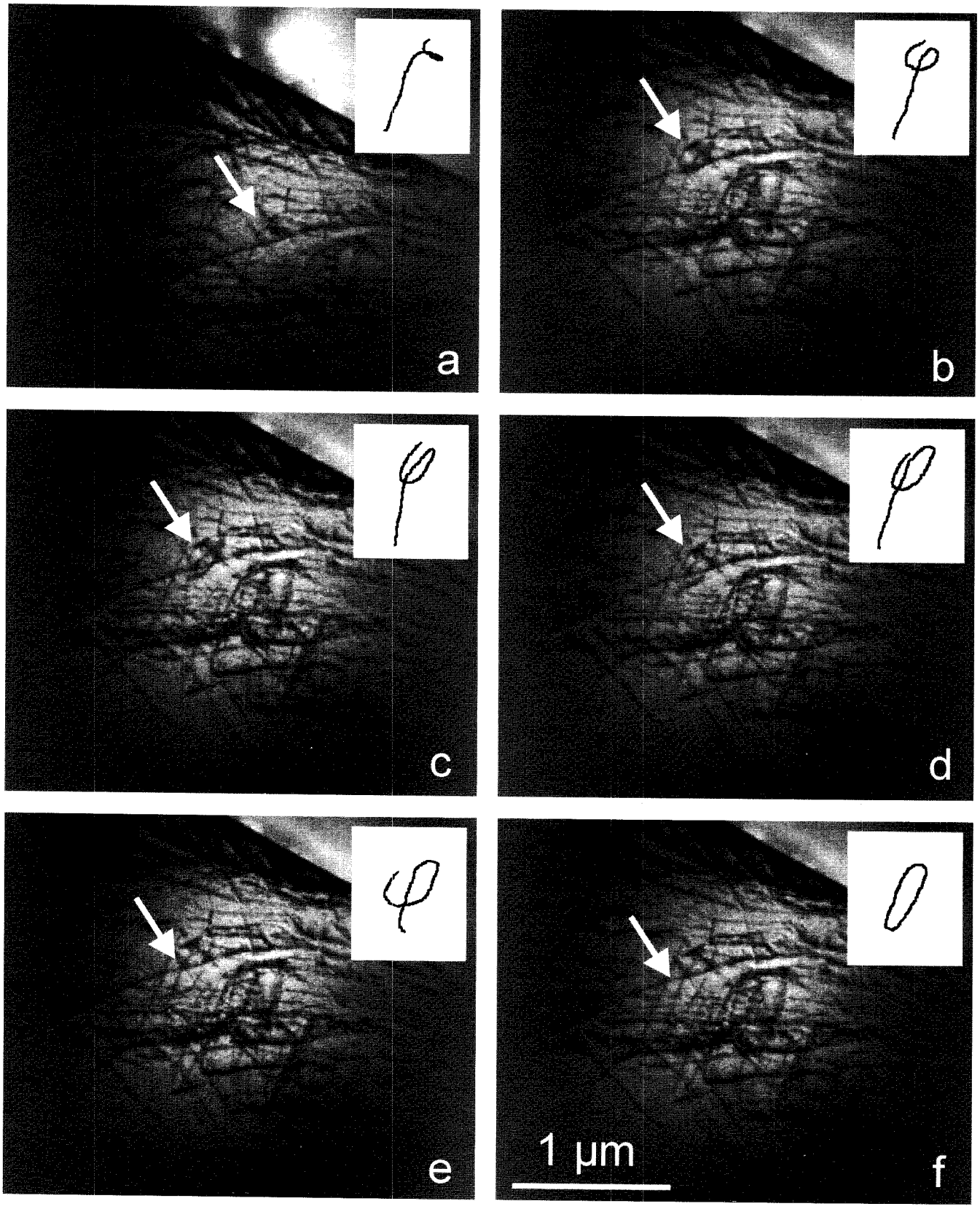

Fig. 16. Several stages of dislocation multiplication in a specimens with OR A2.

fracture J_c amounts to 1684 and 1180 J m^{-2} for orientation relations A and B, respectively [15]. Consequently, a large amount of the plastic work is expended far from the crack tip and is not directly increasing the critical stress intensity factor. This plastic deformation leads to the formation of voids in front of the main crack, so that void formation and coalescence is an essential mechanism of crack extension in the sandwich samples (Figs. 5 and 7).

Owing to the complex stress state near the cracks, dislocations move on all slip systems with orientation factors listed in Table 1 as well as on slip systems with zero macroscopic orientation factors comprising the Burgers vectors contained in the interface plane. The dominating slip planes are of {112} type. Slip is particularly extensive near the crack tip. Mostly, the motion of individual dislocations cannot be resolved there. However, dislocation motion is also observed far away from the crack leading to the large values of the total fracture energy.

Interface fracture is frequently treated as semi-brittle with the emission of dislocations at the crack tip [3, 4]. In the present experiments, the high density of dislocations introduced by the diffusion bonding process prevented the observation of dislocation emission. On the other hand, the present study showed that many dislocations are generated by dislocation multiplication in the plastic zone as during usual plastic deformation. One argument is the observation of dislocations moving towards the crack as in Fig. 15. These dislocations must have been created far from the crack. In addition, dislocation multiplication by the Koehler–Orowan–Gilman mechanism [5–7] was directly imaged. Therefore, it may be concluded that most dislocations carrying the deformation in the plastic zone of the cracks are generated by usual dislocation multiplication.

6. Conclusions

- For the investigated specimens with interfaces possessing high adhesion energies, cracks run along the interfaces but more frequently inside the Nb sheet.
- The cracks are strongly blunted, indicating extensive plastic deformation in the Nb. Fracture energies calculated from the crack opening displacement are between the work of adhesion and the fracture energies determined by macroscopic fracture tests.
- Dislocations move on slip systems with both high and zero orientation factors corresponding to the macroscopic tensile loading, preferentially on {112} planes.
- Most dislocations are created by the double-cross slip multiplication mechanism.

The authors thank Prof. Frank Ernst for his contribution to the project application. They acknowledge technical help by Rosamunde Möhner and Ute Salzberger. They are grateful to the Deutsche Forschungsgemeinschaft (DFG) for financial support.

References

[1] F. Ernst: Mater. Sci. Eng. R 14 (1995) 97.
[2] J.R. Rice, R. Thomson: Phil. Mag. 29 (1974) 73.
[3] J. Rice, Z. Suo, J.S. Wang, in: M. Rühle, A.G. Evans, M.F. Ashby, J.P. Hirth (Eds.), Metal-Ceramic Interfaces, Acta Scripta Metall. Proc. Ser., Vol. 4, Pergamon, Oxford (1990) 269.
[4] G.E. Beltz, J.R. Rice: Acta Metall. Mater. 40 (1992) S321.
[5] J.S. Koehler: Phys. Rev. 86 (1952) 52.
[6] E. Orowan, in: Dislocations in Metals, Am. Inst. Mining and Metallurg. Eng., New York (1954) 103.
[7] W.G. Johnston, J.J. Gilman: J. Appl. Phys. 31 (1960) 632.
[8] D. Korn, G. Elssner, H.F. Fischmeister, M. Rühle: Acta Metall. Mater. 40 (1992) S355.
[9] G. Elssner, D. Korn, M. Rühle: Scripta Metall. Mater. 31 (1994) 1037.
[10] D. Korn, G. Elssner, R.M. Cannon, M. Rühle: Acta Mater. 50 (2002) 3881.
[11] R.M. Cannon, D. Korn, G. Elssner, M. Rühle: Acta Mater. 50 (2002) 3903.
[12] M.S. Duesbery, R.A. Foxall: Phil. Mag. 20 (1969) 719.
[13] U. Messerschmidt, F. Appel: Ultramicroscopy 1 (1976) 223.
[14] A.G. Atkins, Y.-W. Mai: Elastic and Plastic Fracture, Ellis Horwood Publ., Chichester (1985).
[15] M. Bartsch, Z.-F. Zhang, C. Scheu, M. Rühle, U. Messerschmidt: Fracture parameters of chevron-notched Al_2O_3/Nb sandwich specimens, Z. Metallkd. 95 (2004) 781.
[16] G. Soyez: PhD Thesis, University of Stuttgart (1996).
[17] G. Soyez, G. Elssner, M. Rühle, R. Raj: Acta Mater. 46 (1998) 3571.
[18] G. Soyez, G. Elssner, M. Rühle, R. Raj: J. Mater. Sci. 35 (2000) 1087.
[19] R.O. Ritchie, R.M. Cannon, B.J. Dalgleish, R.H. Dauskardt, J.M. McNaney: Mater. Sci. Eng. A 166 (1993) 221.
[20] J.M. McNaney, R.M. Cannon, R.O. Ritchie: Int. J. Fracture 66 (1994) 227.
[21] J.J. Dundurs: J. Appl. Mech. 36 (1969) 650.
[22] M. Jilavi: Thesis, University of Stuttgart (1994).

(Received June 1, 2004; accepted July 6, 2004)

Correspondence address

Prof. U. Messerschmidt
MPI für Mikrostrukturphysik
Weinberg 2, D-06120 Halle (Saale), Germany
Tel.: +49 345 5582 927
Fax: +49 345 5511 223
E-mail: um@mpi-halle.de